Applications of Cloning Algorithm to Soil-Structure Interaction Analysis

Ken'Ichi Moriyama
Taisei Corporation, Tokyo, Japan

ABSTRACT

A soil-structure interaction analysis method is presented. The system is devided into two subsystems which are the near- and far-fields. The near-field is modeled by Finite Element Method to represent irregular soil region, foundations and superstructures. The far-field is the elastic unbounded region which is represented in the form of boundary(freuency dependent) impedance matrix according to a cloning algorithm. Soil-structure interaction systems are analyzed to show the efficiency of the cloning algorithm and to capture their dynamic respnse characteristics.

INTRODUCTION

It is important to take the soil-structure interaction effect into consideration in performing dynamic response analysis of large structure such as nuclear power plant. With rapid increase of computing power, even three dimensional analysis can be conducted in redent years. Though the Finite Element Method is commonly used to represent irregular soil region, (embedded) foundations and superstructures, such special techniques as transmitting boudary (Lysmer et al, 1975), infinite element (Medina et al, 1983), hybrid method (Gupta et al, 1981), Boundary Element Method (Yamashita et al, 1987), flexble volume method (Tabatabaie, 1982), are employed to accomplish radiation condition. In this paper, unbounded soil region is represented in the form of a (frequency dependent) boundary impedance matrix according to a cloning algorithm (Dasgupta, 1982). The cloning algorithm needs no analytical formulation and uses only the conventional finite element formulation involving matrix invertion and eigenvalue-related calculation. Two dimensional analysis were presented by Moriyama et al (1988).Three dimensional impedance functions for a foundation are calculated in this paper.

ANALYSIS METHODOLOGY

Euation of Motion

Following the substructure method (Wolf, 1985), a soil-structure interaction system is devided into two subsystems the near- and far-fields. To take advantage of versatility in modeling, the near-field is represented with finite elements. The far-field is represented as the boundary impedance matrix which is calculated according to the cloning algorithm (Dasgupta, 1982). The equation of motion of the soil-structure interaction system in frequency domain is written as follows:

$$\left[-\omega^2\begin{bmatrix} M_{ss} & M_{si} \\ M_{is} & M_{ii} \end{bmatrix} + \begin{bmatrix} K_{ss} & K_{si} \\ K_{is} & K_{ii}+K_i^* \end{bmatrix}\right]\begin{Bmatrix} u_s \\ u_i \end{Bmatrix} = \begin{Bmatrix} f_s \\ K_i^*\hat{u}_i \end{Bmatrix} \qquad (1)$$

where

i : Degree of freedom on boundary.

s : Degree of freedom other than i.

M_{jl} : Mass submatrix with j,l degree-of-freedom.

K_{jl} : Stiffness submatrix with j,l degree-of-freedom.

f_i : External force vector.

u_j : Absolute displacement vector corresponding to j degree-of-freedom.

K^*_i : Boundary matrix of far-field.

$\hat{u}_i$: Absolute displacement of soil with excavation(for ground excitation).

Boundary Impedance Matrix of the Far-Field

The boundary impedance of the far-field is obtained by using a cloning algorithm (Dasgupta, 1982) which concieves the unbounded region as a summation of infinite number of geometrically similar cells. The boundary impedance for the unbounded region is computed from the dynamic stiffness matrix pertaining to a cell.

NUMERICAL RESULTS AND DISCUSSIONS

To verify accuracy of the boundary impedance from the cloning algorithm and numerical procedure, the impedance functions for a circular foundation on an elastic half space are calculated and compared with the results by Day (1977). The model is shown in Fig.1. The viscous boundary is attached at the bottom of the model and the boundary impedance matrix from the cloning algorithm is attached at the side. Following the expression of Day (1977), the impedances K_{ii}, the stiffness coefficients k_{ii} and the damping coefficients c_{ii} are introduced. These are defined as follows:

$$K_{HH}=Ga\left(k_{HH}+i\frac{2\pi fa}{V_s}c_{HH}\right) \qquad (2.a)$$

$$K_{RR}=Ga^3\left(k_{RR}+i\frac{2\pi fa}{V_s}c_{RR}\right) \qquad (2.b)$$

$$K_{VV}=Ga\left(k_{VV}+i\frac{2\pi fa}{V_s}c_{VV}\right) \qquad (2.c)$$

$$K_{TT}=Ga^3\left(k_{TT}+i\frac{2\pi fa}{V_s}c_{TT}\right) \qquad (2.d)$$

G : Shear modulus of soil.
a : Radius of circular foundation.
f : Frequency of exciting force.

Obtained impedance functions are shown in Fig.2. Comparison with the results by Day (1977) shows that the stiffness coefficients fluctuates a little but the damping coefficients show good agreement. The horizontal impedance functions, whict are from cloning algorithm and using viscous boundary at the side of the model instead of the boudary impedance matrix from the cloning algorithm, are shown in Fig.3. The impedance function with side viscous boundary gives bigger stiffness coefficient and fluctuating damping coefficient. From these results, it can be seen that the boundary impedance matrix from cloning algorithm represents radiation damping properly.

The rocking impedance functions for a circular foundation on layered half space are shown in Fig.4. The model shown in Fig.1 is used. The shear velocity of surface layer is 400m/sec and the thickness of surface layers are 0m (uniform), 20m and 40m. The viscous boundary is attached at the bottom and the boundary impedance of layered half space is attached at the side. The stronger frequency dependence for layered half space can be seen than for half space and its tendency becomes greater for thicker suface layer. It is also found that the damping is small for thin surface layer.These characteristics coincide with the results by Luco (1974).

The rocking impedance for three different embedded foundations with 40m surface layer are shown in Fig.5. The soil model is the same as in Fig.1. The broken line in Fig.5 is the impedance function without embedment. It can be seen that embedment makes impedance a little stiffer in low frequency range and damping very different from that of foundation without embedment. Therefore, it is anticipated that the shape of boundation affects the impedance function very much.

Fig.7 shows the torsional and vertical impedances for an embedded foundation. The model is shown in Fig.6 and three embedment depth (0m, 20m and 40m) are examined. Inaccuracy is found for the impedance for deep embedded foundation from comparison with the results by Day (1977). It may be caused by the size of model and/or the used finite element.

CONCLUSIONS

The impedance functions for the various foundation types are calculated for an elastic half space and layered half space and compared with published results. The results show the effectiveness of the cloning algorithm for both half space and layered half space. The soil-structure interaction effects can be taken into account for the engineering design purpose even under complicated site and foundtion condition by using the cloning algorithm.

REFERENCES

Dasgupta, G., (1982) Finite Element Formulation for Unbounded Homogeneous Continua. Journal of Applied Mechanics, (ASME), Vol. 49, pp. 136-140.

Day, S.M., (1977) Finite Element Analysis of Seismic Scattering Problems. Ph.D. Thesis, University of California, San Diego.

Gupta, S. and Penzien, J., (1981) Hybrid Modeling of Soil-Structure Interaction for Embedded Structures. Proceedings of 6th. SMiRT.

Luco, J.E., (1974) Impedance Functions for a Rigid Foundation on a Layered Medium. Nuclear Engineering and Design, Vol.31, pp. 204-217.

Lysmer, J., Udaka, T., Tsai, C.-F. and Seed, H.B. (1975) FLUSH-A Computer Program for Approximate 3-D Analysis of Soil-Structure Interaction Problems. EERC Report UCB/EERC-75/30, University of California, Berkley.

Medina, F. and Taylor, R.L. (1983) Finite Element Techniques for Problems of Unbounded Domains. International Journal for Numerical Methods in Engineering, Vol.19, pp.1209-1226.

Moriyama, K., Dasgupta, G. and Shinozuka, M. (1988) Soil-Structure Interaction Analysis by Using Cloning Argorithm. Proceedings of 9th. World Conference on Earthquake Engineering. Vol.III, PP.349-354.

Tabatabaie-Raissi, M., (1982) The Flexble Volume Method for Dynamic Soil-Structure Interaction Analysis. Ph.D. Thesis, University of California, Berkeley.

Wolf, J.P., (1985) Dynamic Soil-Structure Interaction. Prentice Hall Inc.

Yamashita, T., Tanaka, H., Miura, K., Ueno, K., Motosaka, M. and Kanda, K., (1987) Study on the Dynamic Cross Interaction for the Embedded Structures. Proceedings of 9th. SMiRT.

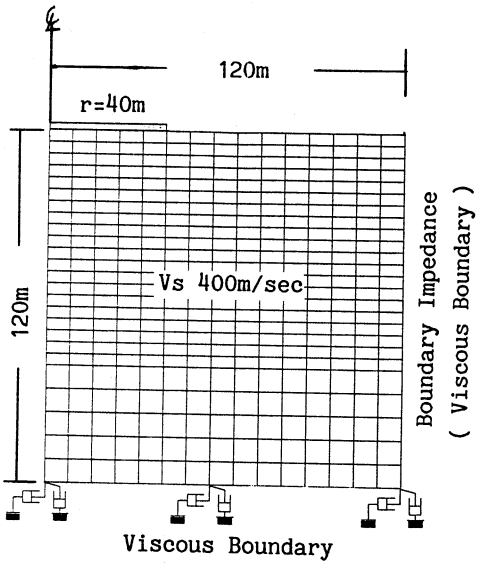

Fig.1 Model.

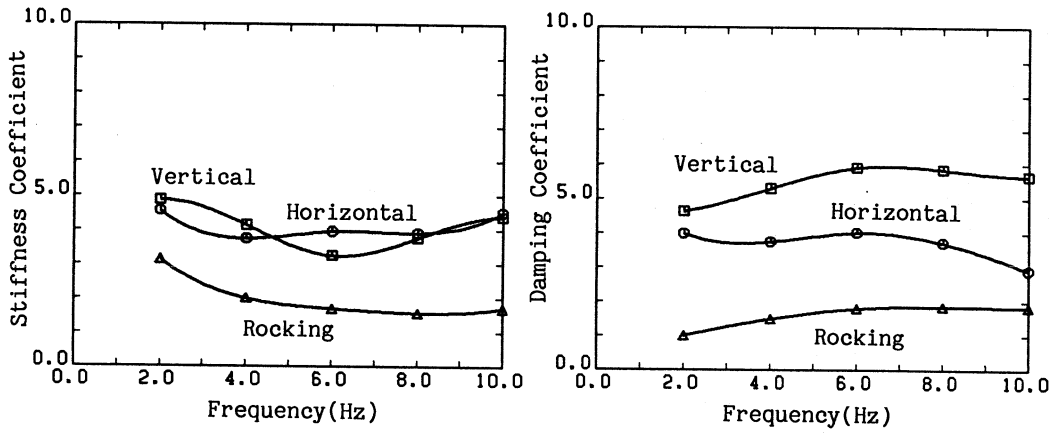

Fig.2 Impedance Functions for a Circular Foundation on an Elastic Half Space.

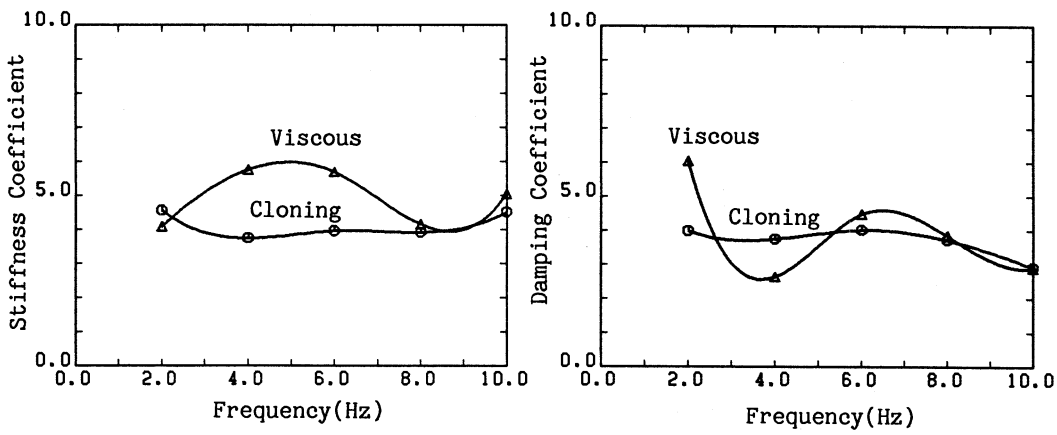

Fig.3 Horizontal Impedance Functions for a Circular Foundation on an Elastic Half Space.

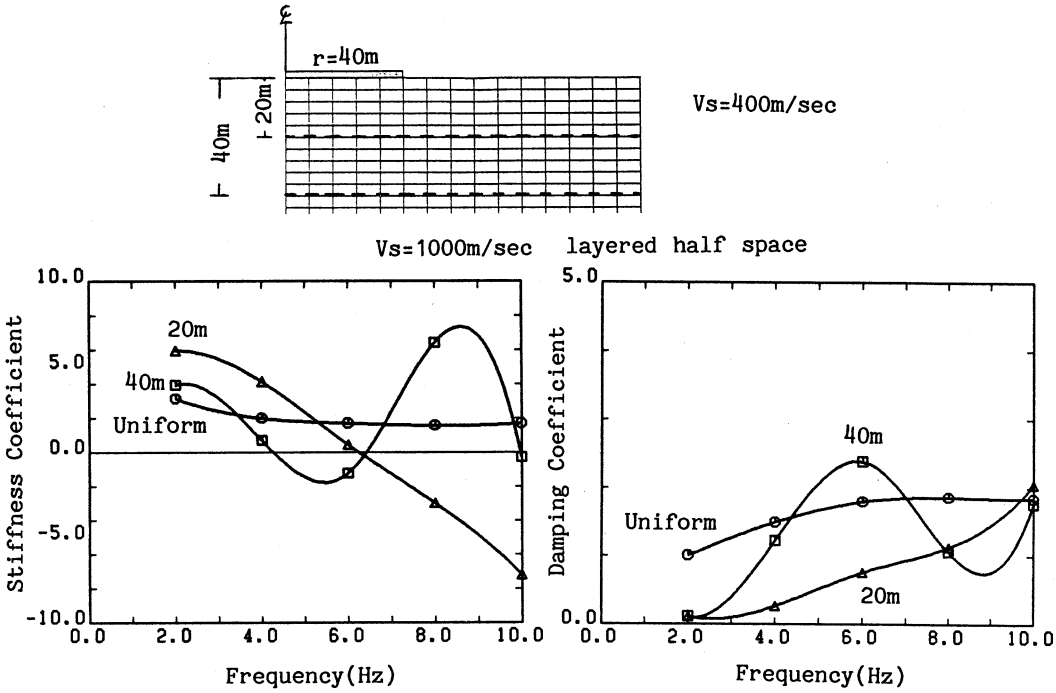

Fig.4 Rocking Impedance Functions for a Circular Foundation on a Layered Half Space.

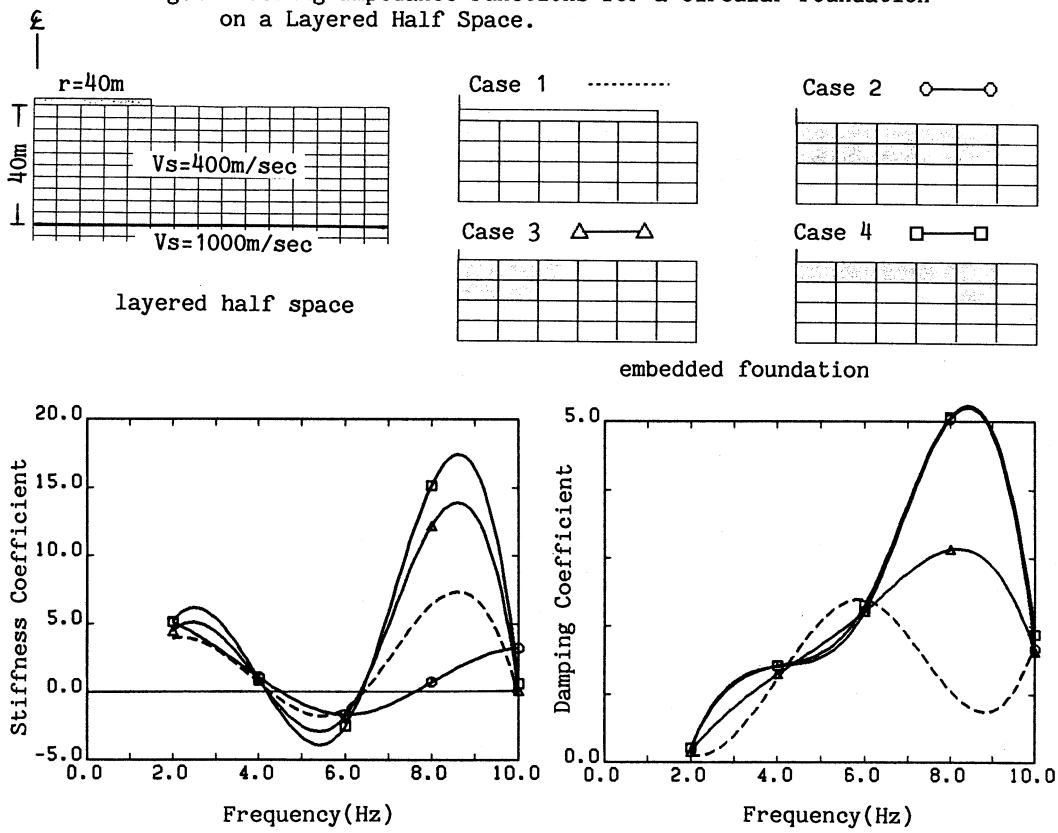

Fig.5 Rocking Impedance Functions for Various Embedded Foundation.

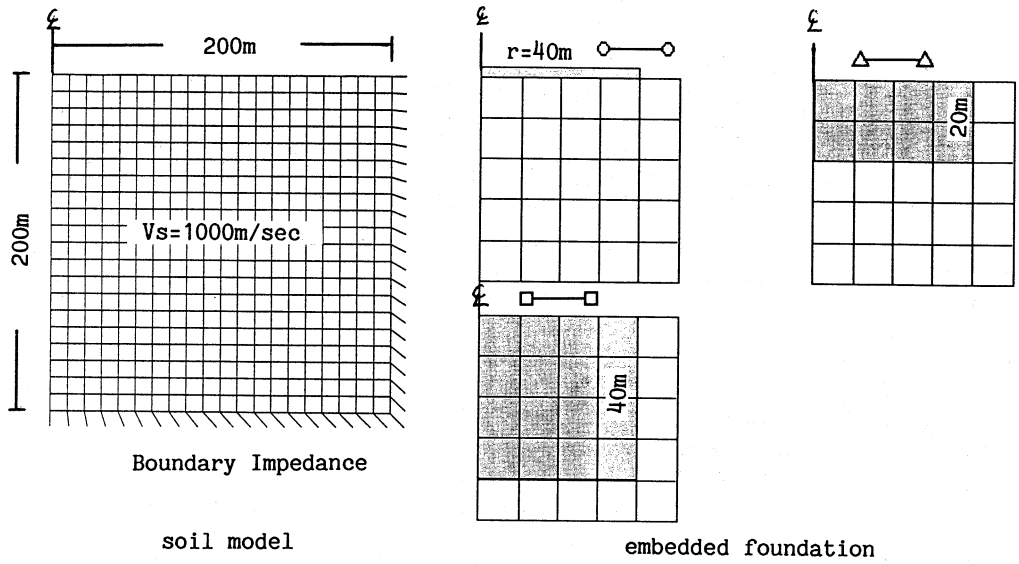

Fig.6 Model.

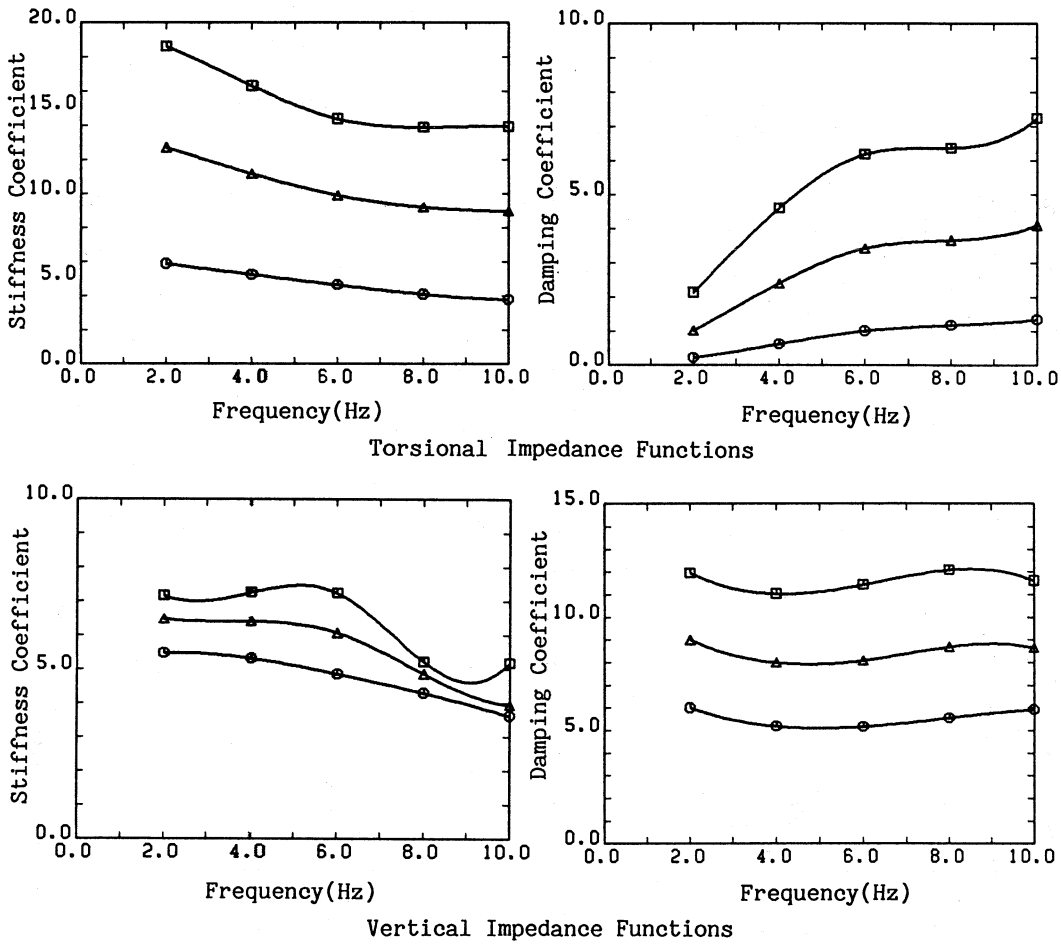

Fig.7 Torsional and Vertical Impedance Functions for a Embedded Foundation.

The Effect of Embedment Depth on Seismic Response of a Nuclear Reactor Building Design

F. Ostadan, W. S. Tseng, P. S. Sawhney
Bechtel Power Corporation, San Francisco, CA USA
A. S. Liu
General Electric Company, San Jose, CA USA

INTRODUCTION

Selection of embedment depth of a nuclear reactor building is based on various design, construction, maintenance and operation considerations. Increasing the embedment depth of the reactor building reduces the seismic responses of the building leading to lower seismic loads and floor acceleration responses. The seismic response reduction resulting from increasing the embedment depth must be weighed against other considerations in order to optimize the design. In this study seismic soil-structure interaction (SSI) responses of a reactor building of a standard plant with two embedment depths of 12m (20% of building height) and 26m(40% of building height) are investigated. Since the standard plant is designed for a wide range of potential sites, studies are made for three sites with properties ranging from soft to medium stiff to hard rock sites.

STANDARD PLANT STRUCTURES

The site plan of a standard plant is shown in Fig. 1. The plant consists of three main buildings: the reactor, control, and turbine buildings. The cross section of the plant along the x-axis based on 26m embedment design is shown in Fig. 2. For the purpose of SSI analyses, stick models are used to model the buildings and their internal structures. The stick model used for the reactor building is shown in Fig. 3. For the design with deep embedment (26m), seismic SSI responses of the reactor building including structure-to-structure interaction effects in three generic sites are evaluated and compared in Ref. 1. The study in Ref. 1 shows that through soil structure-to-structure interaction effect is a secondary SSI effect for the reactor building considered and does not change the SSI responses significantly. It is also shown that 2-D and 3-D SSI analyses result in similar response magnitude and characteristic for the cases investigated. Thus, to evaluate the effect of variation in embedment depth, 2-D SSI models of the reactor building are used to compute the responses. Only the analyses results for horizontal x-direction are presented in this paper.

SEISMIC DESIGN CRITERIA AND ANALYSIS METHODOLOGY

The seismic design response spectrum for the horizontal input motion is based on the smooth, broad-band NRC RG 1.60 response spectrum scaled to maximum acceleration of 0.15g. The response spectrum of input motion is compared with RG 1.60 spectrum for 2% damping in Fig. 4. The input motion is prescribed at the finished grade in the free-field. The motion is assumed to be generated by vertically propagating shear waves. The damping values for structural components are in accordance with the RG 1.61 recommendations. The soil

material damping values are the strain-compatible soil damping values obtained from the free-field site response analysis. The nonlinearities in soil shear modulus and damping are considered by using strain-compatible properties obtained from free-field analysis using computer program SHAKE (Ref. 2). Computer program SASSI (Ref. 3) is used to obtain SSI responses.

SITE SOIL PROPERTIES AND SSI ANALYSIS CASES

From the wide range of soil profiles considered for the standard plant seismic analysis, three sites are selected for the present study. The initial and strain-compatible shear wave velocity profiles for these three sites obtained from SHAKE analyses are shown in Fig. 5. The UB, VP, and HR profiles represent the soft, medium stiff and hard rock sites. The UB and VP profiles extend to the depth of 46m and are underlaid by hard rock. The HR Profile represents a uniform halfspace. As expected, the softening effect due to induced shear strain is larger for the softer soil profiles. For the HR profile the reduction is insignificant and the initial low-strain properties are practically maintained. Using the strain-compatible soil properties, SSI analyses are performed in horizontal x-directions for 6 cases as identified in Table 1. Cases in Group A represent the 12m embedment depth cases in the three sites. Cases in Group B represent the corresponding SSI cases for 26m embedment depth. SASSI 2-D SSI models of the reactor building are shown in Figs. 6a and 6b.

RESULTS AND COMPARISONS

Results of analysis in terms of acceleration response spectra at the top of reactor building (Node 95 in Fig. 3) for SSI analysis cases of Group A and Group B are compared in Figs. 7 and 8 to evaluate the effect of site soil properties on the response. As shown in these figures, for both 12m and 26m embedment depths, the SSI responses at the hard rock site dominate the responses at the other two sites. Irrespective to the embedment depth, the lowest SSI response is obtained in the softest site. This is due to considerable reduction of motion in the free-field with depth that results for the soft site. Because of this reduction, the embedded part of the reactor building is subjected to reduced effective translational motion at the soft site. The increased rocking motion is not significant. Change in the SSI frequency due to the change in the soil properties for different site conditions can be clearly identified in Figs. 7 and 8.

To show the effect of variation in embedment depth on the SSI responses for each site, response spectra at the top of the reactor building (Node 95 of Figure 3) are compared in Figs. 9, 10, and 11. As shown in these figures, the reduction of the embedment depth reduces and SSI frequency and increases the response. For each site, the increase in the response due to reduction of embedment depth can be attributed to the increase in the effective input motion for the foundation and the increase in the free-standing height of the building resulting from reduction of embedment depth.

The results of analysis in terms of maximum moment and shear along the height of the reactor building for cases in Group A (see Table 1) are compared in Fig. 12. Similar to the trend observed for the acceleration responses, the maximum loads are governed by the hard rock.

To evaluate the effect of embedment depth on seismic loads, maximum loads for the governing cases of E10X (12m embedment) and C10X (26m embedment) in the hard rock site are compared in Fig. 13. The maximum moment and shear along the height of the building from top to the grade level of C10X Case are very close. Below this level, the maximum loads decrease for C10X case; whereas they continue to increase for the case of E10X up to the grade level of

E10X case, beyond which the loads again are reduced. Thus, the reactor building with 12m embedment depth is subjected to much larger loads at the building base as compared to the loads for the 26m embedment.

CONCLUSION

The comparison of the seismic responses of the reactor building for 12m and 26m embedment depths shows that both the acceleration response spectra and maximum seismic loads increase as the embedment depth is reduced. The increase of seismic response occurs for all three sites investigated. The increase in response is due to increases in the free-standing height of the building and in effective foundation input motions that result from the reduction of embedment depth. Results of the study show that the maximum seismic shear of the reactor building occurs at grade level and decreases below grade. The maximum seismic moment does not change significantly along the embedded height of the building. Thus, the reduction of embedment depth from 26m to 12m results in significant increase in the maximum seismic load for the building at the grade level.

ACKNOWLEDGMENTS

This work was supported by Electric Power Research Institute (EPRI) under contract number RP266-05.

REFERENCES

Ostadan, F., Tseng W., Liu, A. S., 1989. "Effect of Site Soil Proferties on Seismic SSI Response of Embedded Structures," ASCE Foundation Engineering Congress, Evanston, Illinois, June.

Schnabel, PB., Lysmer, J., Seed, H. B., 1972. "SHAKE - A Program for Earthquake Response Analysis of Horizontally Layered Sites, "EERC Report 72-12, University of California, Berkeley.

Lysmer, J., Tabatabaie-Raissi, M., Ostadan, F., Tajirian, F., Vahdani, S., 1981. "SASSI - A System for Analysis of Soil-Structure Interaction," Report UCB/GT/81-02, University of California, Berkeley, Berkeley, CA.

Table 1. SSI Analyses Cases

Velocity Profile	Group A (12m Embedment)	Group B (26m Embedment)
UB	E2X	C2X
VP	E4X	C4X
HR	E10X	C10X

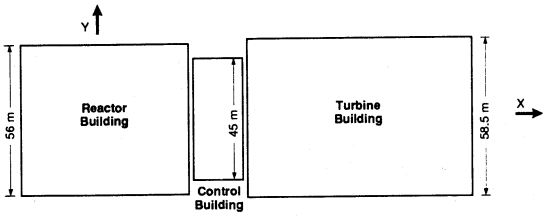

Figure 1. Standard Design Site Plan

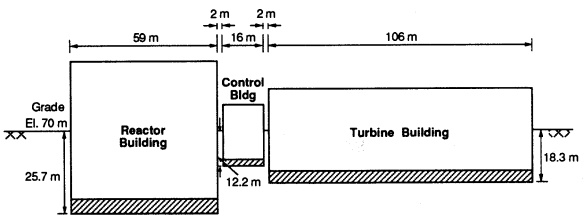

Figure 2. X-Direction Section View

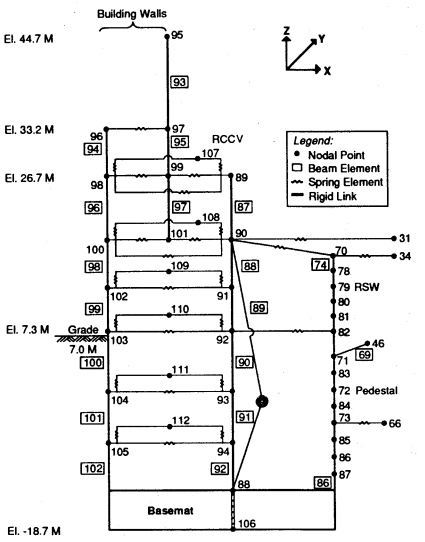

Figure 3. Reactor Building Stick Model

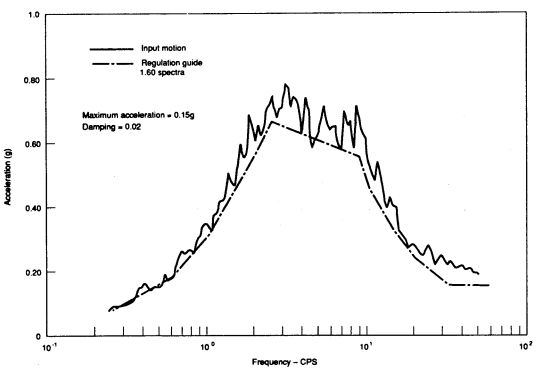

Figure 4. Response Spectrum of Design Motion

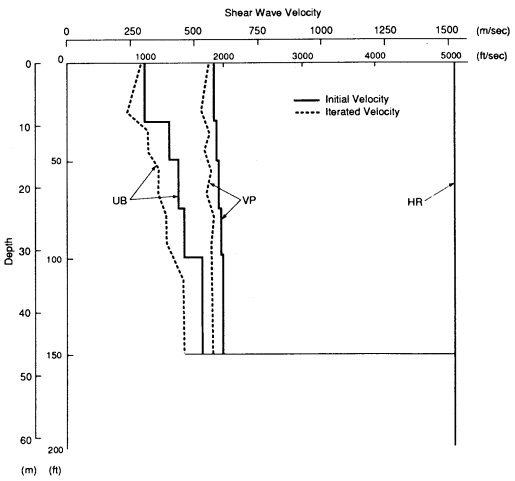

Figure 5. Initial and Iterated Shear Wave Velocity Profile

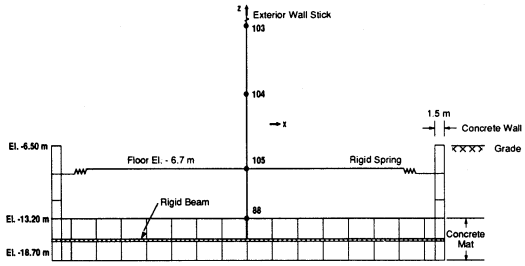

Figure 6a. Reactor Building SASSI SSI Model – 12 m Embedment Depth

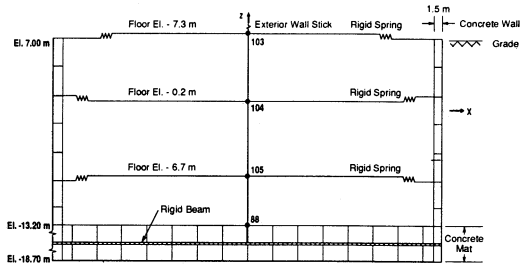

Figure 6b. Reactor Building SASSI SSI Model – 26 m Embedment Depth

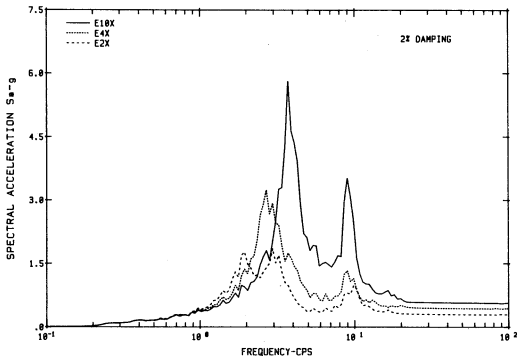

Figure 7. Comparison of Responses at Node 95 (Group A Cases)

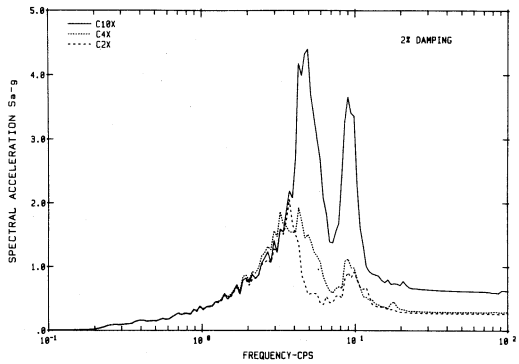

Figure 8. Comparison of Responses at Node 95 (Group B Cases)

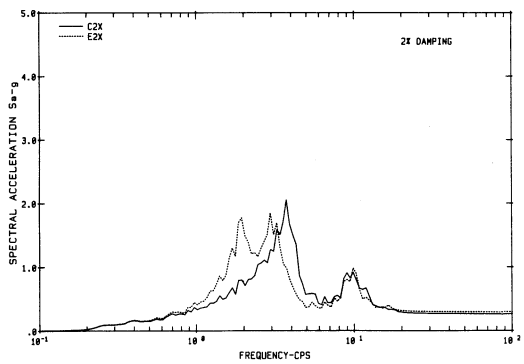

Figure 9. Comparison of Responses at Node 95 (C2X vs E2X)

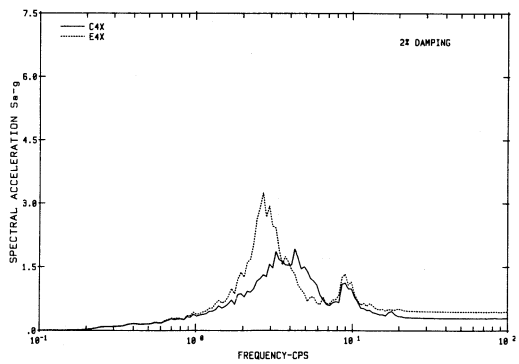

Figure 10. Comparison of Responses at Node 95 (C4X vs E4X)

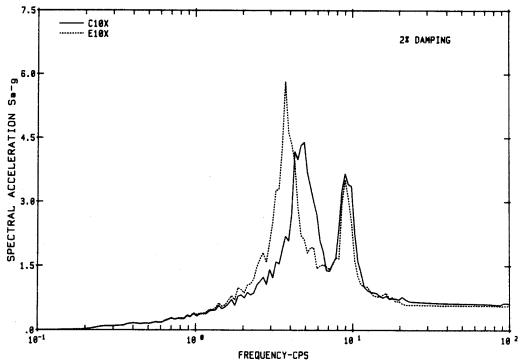

Figure 11. Comparison of Responses at Node 95 (C10X vs E10X)

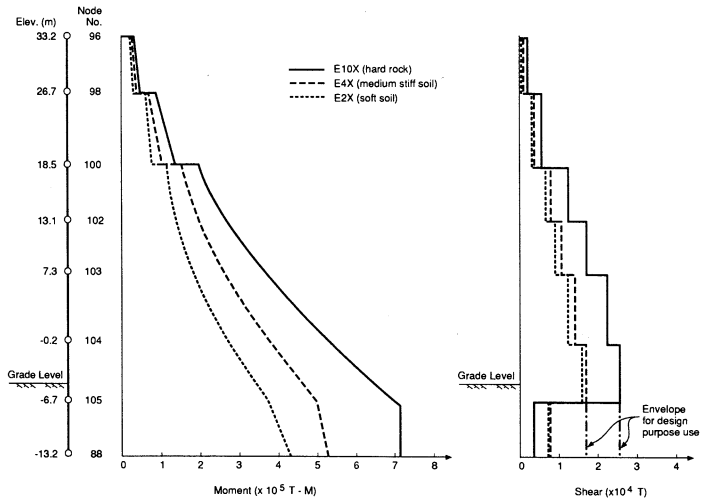

Figure 12. Comparison of Moment and Shear Along the Reactor Building Wall (12 m Embedment)

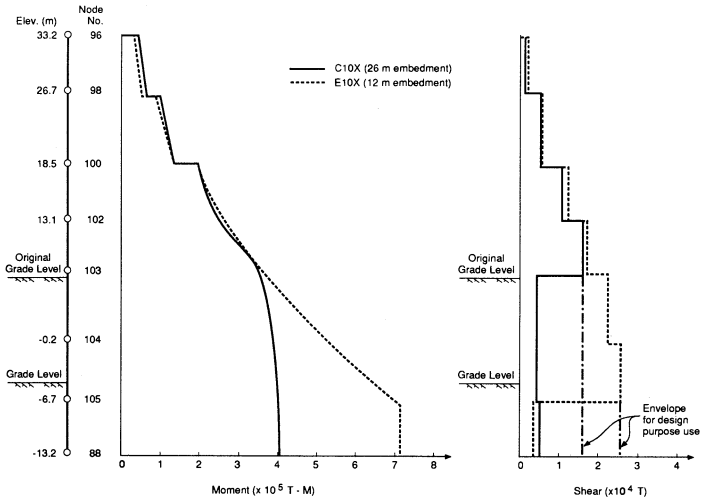

Figure 13. Comparison of Moment and Shear Along the Reactor Building Wall (Hard Rock Site)